Collective excitations in itinerant spiral magnets

A. P. Kampf
Institut für Theoretische Physik, Universität zu Köln, Zülpicher Strasse 77, 50937 Köln, Germany
(Received 2 June 1995)

We investigate the coupled charge and spin collective excitations in the spiral phases of the two-dimensional Hubbard model using a generalized random-phase approximation. Already for small doping the spin-wave excitations are strongly renormalized due to low-energy particle-hole excitations. Besides the three Goldstone modes of the spiral state the dynamical susceptibility reveals an extra zero mode for low doping and strong coupling values signaling an intrinsic instability of the homogeneous spiral state. In addition, near-zero modes are found in the vicinity of the spiral pitch wave number for out-of-plane spin fluctuations. Their origin is found to be the near degeneracy with staggered noncoplanar spiral states which, however, are not the lowest energy Hartree-Fock solutions among the homogeneous spiral states.

I. INTRODUCTION

A lot of attention has been focused on the strongly interacting electron problem in recent years since the discovery of cuprate superconductors. While the magnetic properties of the insulating parent compounds may be understood in terms of an antiferromagnetic (AF) two-dimensional Heisenberg model or a Hubbard model at half-filling on a square lattice low doped metallic samples still pose many puzzles. Theoretical studies based on t-J or Hubbard models have attempted to explore the properties of a small amount of carriers doped into an antiferromagnet. Both the magnetic correlations and the dynamics of the carriers in low doped antiferromagnets remain two key issues for a theoretical understanding of cuprate superconductors.

Early on Shraiman and Siggia pointed out that holes moving in an AF environment give rise to a long range dipolar distortion of the staggered magnetic order.[1] In particular, a spiral twist of the magnetization was suggested as a compromise spin structure in which the doped holes can gain kinetic energy without too much cost in magnetic energy. Subsequently mean-field theories have been developed to determine the favorable homogeneous spiral states for the square lattice Hubbard or t-J model.[2–8] Homogeneous spiral states for the square lattice at small doping appear to be unstable towards phase separation into hole-rich and hole-poor regions as signalled by a negative mean-field compressibility $\partial n/\partial \mu < 0$.[5,9,10] Alternatively, domain wall structures have been proposed as possibly favorable inhomogeneous states at low doping.[11–13] The inclusion of longer range Coulomb interactions is expected to prevent phase separation and stabilize a homogeneous state. Although phase separation is a *bona fide* possibility for the ground state of the Hubbard model, the real electrons in a doped antiferromagnet will most likely favor a translational invariant state. In this sense spiral spin textures offer a compromise structure for the competing kinetic and magnetic energies.

Recently, attention has also been given to the spin dynamics and the collective excitations in the spiral state of the doped Hubbard model. A commensurate spin density wave (SDW) state has two degenerate transverse Goldstone modes. General symmetry arguments imply that in a coplanar spiral spin texture the spin-wave excitation spectrum has three Goldstone modes located at $\mathbf{0}, \pm\mathbf{Q}$, where $\mathbf{Q}$ is the spiral pitch wave vector.[14–16] One of these modes is related to the spin rotation in the plane of the spiral, and two Goldstone modes follow from the rotation of the spiral plane itself. The motion of doped holes is, however, closely coupled to the magnetic structure they are moving in and therefore the overall dispersion of the spin waves is renormalized by the continuum of particle-hole excitations.[17,18]

Neutron scattering experiments on $La_{2-x}Sr_xCuO_4$ have found incommensurate magnetic fluctuations in the dynamical susceptibility $\mathrm{Im}\chi(\mathbf{q},\omega)$.[19] This is one of the reasons why spiral magnetic states have received a particular interest. However, the mean-field spiral states maintain long range magnetic order which is not realized in the doped copper oxide superconductors. A detailed investigation of the quantum fluctuations is therefore in order to explore the relevance of spiral states for cuprates.

Yet, other materials may provide a realization of a metallic spiral state. For example, recent neutron scattering experiments have detected an incommensurate, spiral SDW in the metallic Mott-Hubbard system $V_{2-y}O_3$ in which the carrier density is determined by the vanadium deficiency.[20] Similarly, a spiral state has been proposed to describe the perovskite manganese oxides $La_{1-x}(Ba,Ca,Sr)_xMnO_3$ for small x.[21] While a detailed description of these intriguing materials may require to take into account their crystal structure and more than one relevant atomic orbital, a general description of the collective excitations in a spiral state may find its application for a number of different model systems.

For this purpose we set up in this paper a convenient generalized random phase approximation (GRPA) scheme to analyze the dynamics of spin and charge excitations. Although the results can be straightforwardly extended to various lattice structures, we specifically calculate the dynamical susceptibilities for the spiral states of the square lattice, single band Hubbard model. This allows us to relate our results to a number of recent works and to provide further insight into the apparent instabilities of homogeneous spiral spin structures. In Sec. II we review the mean-field theory for coplanar spiral phases in the Hubbard model. In Secs. III and IV we derive diagrammatically the dynamical spin and

charge susceptibilities and analyze the collective excitation spectrum in Sec. V. An extension of the mean-field theory to noncoplanar spiral states as recently suggested by Chubukov and Musaelian[22] is given in Sec. VI. Finally, we summarize our conclusions in Sec. VII.

II. HARTREE-FOCK SPIRAL STATES

We study the single band Hubbard Hamiltonian

$$H=-\sum_{ij,\sigma} t_{ij}(c^{\dagger}_{i\sigma}c_{j\sigma}+\text{H.c.})+U\sum_{i} n_{i\uparrow}n_{i\downarrow} \tag{1}$$

on the square lattice. In the standard notation $c_{i\sigma}$ ($c^{\dagger}_{i\sigma}$) annihilates (creates) an electron with spin σ at lattice site i and $n_{i\sigma}=c^{\dagger}_{i\sigma}c_{i\sigma}$ is the particle number operator. The hopping amplitude is restricted to nearest-neighbor (t) and next-nearest-neighbor sites (t'). At half-filling the ground state is a two-sublattice antiferromagnet for t' smaller than a critical, U dependent value[23] which is conveniently described in the SDW formalism of Schrieffer, Wen, and Zhang.[24] Away from half-filling incommensurate spiral states appear as Hartree-Fock ground states with a wave number $\mathbf{Q}$ that for a small concentration of holes continuously moves away from (π,π) with increasing doping.[1,8,25]

In order to analyze the mean-field spin structures we rotate locally the spin quantization axis by the unitary transformation

$$d_{i\sigma}=\sum_{\sigma'} [e^{i\sigma_y\theta_i/2}]_{\sigma\sigma'}c_{i\sigma'} \tag{2}$$

which leaves the Hubbard interaction unchanged. In the new spin reference frame the Hubbard Hamiltonian reads

$$H=-\sum_{ij,\sigma_1\sigma_2} t_{ij}([e^{i\sigma_y\theta_{ij}/2}]_{\sigma_1\sigma_2}d^{\dagger}_{i\sigma_1}d_{j\sigma_2}+\text{H.c.})$$

$$+U\sum_{i} d^{\dagger}_{i\uparrow}d_{i\uparrow}d^{\dagger}_{i\downarrow}d_{i\downarrow} \tag{3}$$

with $\theta_{ij}=\theta_i-\theta_j$. In the following we focus on homogeneous coplanar spiral states for which $\theta_i=\mathbf{Q}\cdot\mathbf{R}_i$ defining the spiral wave number $\mathbf{Q}$. Assuming a ferromagnetic spin alignment in the rotated spin reference frame with a uniform charge density we factorize the Hubbard interaction introducing the site independent electron density n and magnetization m by $\langle n_{i\sigma}\rangle=\langle d^{\dagger}_{i\sigma}d_{i\sigma}\rangle=\frac{1}{2}n+\sigma m$. This corresponds to a spiral spin order in the original spin reference frame of the form $\langle\mathbf{S}_i\rangle=m(\sin\theta_i,0,\cos\theta_i)$. The commensurate SDW state is therefore included for $\mathbf{Q}=(\pi,\pi)$ with the origin of the Brillouin zone shifted to $(\pi/2,\pi/2)$.

The diagonalization of the factorized Hamiltonian leads to the mean-field energy[26]

$$E_{\mathrm{MF}}=\sum_{\mathbf{k}} (E^{-}_{\mathbf{k}}f^{-}_{\mathbf{k}}+E^{+}_{\mathbf{k}}f^{+}_{\mathbf{k}})+NU(\tfrac{1}{4}n^2+m^2) \tag{4}$$

with the $\mathbf{k}$ sum extending over the full Brillouin zone. N is the total number of sites and $f^{\pm}_{\mathbf{k}}$ are the Fermi occupation numbers for the mean-field quasiparticle band states with energies

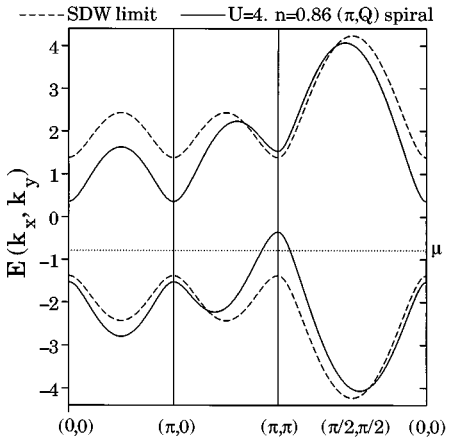

FIG. 1. Representative mean-field quasiparticle dispersion (solid line) in the d-fermion reference for the (π, Q) spiral state for $U/t=4$, $t'=0$, and for a hole concentration of 14%. For comparison, the dashed line shows the dispersion in the commensurate SDW limit at half-filling. The position of the chemical potential is indicated by a dotted line.

$$E^{\pm}_{\mathbf{k}}=\epsilon^{+}_{\mathbf{k}}\pm E_{\mathbf{k}}=\epsilon^{+}_{\mathbf{k}}\pm\sqrt{(\epsilon^{-}_{\mathbf{k}})^2+\Delta^2}. \tag{5}$$

Here, we have defined $\Delta=Um$ and

$$\epsilon^{\pm}_{\mathbf{k}}=\frac{1}{2}\left[\epsilon\left(\mathbf{k}-\frac{\mathbf{Q}}{2}\right)\pm\epsilon\left(\mathbf{k}+\frac{\mathbf{Q}}{2}\right)\right]. \tag{6}$$

$\epsilon(\mathbf{k})\equiv\epsilon(\mathbf{k};t,t')=-2t(\cos k_x+\cos k_y)-4t'\cos k_x\cos k_y$ is the tight binding dispersion for the nearest- and next-nearest-neighbor hopping motion on the square lattice. Δ is determined by the self-consistency condition

$$\frac{2}{U}=\frac{1}{N}\sum_{\mathbf{k}}\frac{f^{-}_{\mathbf{k}}-f^{+}_{\mathbf{k}}}{\sqrt{(\epsilon^{-}_{\mathbf{k}})^2+\Delta^2}}. \tag{7}$$

The spiral wave vector $\mathbf{Q}$ follows from the minimization of the mean-field energy: $\partial E_{\mathrm{MF}}/\partial Q_x=\partial E_{\mathrm{MF}}/\partial Q_y=0$, i.e., from

$$\tan\frac{Q_{x(y)}}{2}\sum_{\mathbf{k}}\cos k_{x(y)}(f^{+}_{\mathbf{k}}+f^{-}_{\mathbf{k}})=\sum_{\mathbf{k}}\frac{\epsilon^{-}_{\mathbf{k}}}{E_{\mathbf{k}}}\sin k_{x(y)}(f^{+}_{\mathbf{k}}-f^{-}_{\mathbf{k}}). \tag{8}$$

The equation for the electron density

$$n=\frac{1}{N}\sum_{\mathbf{k}}(f^{-}_{\mathbf{k}}+f^{+}_{\mathbf{k}}) \tag{9}$$

fixes the chemical potential $\mu(n)$. Equations (7), (8), and (9) have to be solved simultaneously for a self-consistent determination of the Hartree-Fock spiral state parameters. An example for the mean-field quasiparticle dispersion along a closed path in the first Brillouin zone is shown in Fig. 1. The two bands are separated by an indirect gap which closes with increasing hole doping while the chemical potential moves downward in the quasiparticle valence band.

The Hartree-Fock phase diagram has been mapped out in detail previously for $t'=0$ (see, e.g., Ref. 8). Some results have also been reported for finite t'.[27] Since the next-nearest-neighbor hopping removes the particle-hole symmetry of the Hubbard model remarkable differences are found

between hole and electron doping. For example, at strong coupling commensurate spin correlations are stabilized over a finite electron doping range, while hole doping immediately leads to an incommensurate magnetic structure.[27,28]

In the SDW state t' hopping lifts the degeneracy of the dispersion along the magnetic Brillouin zone boundary and the valence band has energy maxima at the four points $\mathbf{k}_p=(\pm\pi/2,\pm\pi/2)$. At finite doping holes will therefore preferentially occupy momentum states near $\mathbf{k}_p$ forming pocketlike features in the Fermi surface of the slightly doped metallic phase. However, even for $t'=0$ quantum fluctuations lead to a maximum for the dispersion of a single hole doped into the half-filled state[29,30] so that the introduction of a finite t' may capture some features of the hole dispersion in the Hubbard model for $t'=0$ even without the inclusion of self-energy corrections. In fact, the existence of hole pockets around the $\mathbf{k}_p$ points has already been taken for granted in some studies of spiral spin states.[11,22]

In solving the mean-field equations for $t'=0$ a diagonal spiral with $\mathbf{Q}=(Q,Q)$ has been found as the lowest energy solution at low doping with a first order transition at a critical hole density to a (π,Q) spiral for weak and intermediate values of U/t.[8] At large U and small doping nearly the whole (Q,Q) spiral region in the phase diagram has a negative compressibility. This indicates that the ground state energy can further be lowered by phase separation; the different hole densities in these phase separated regions are determined by a Maxwell construction for the free energy density.[10]

For hole doping the inclusion of a finite t' hopping modifies these results only quantitatively. At weak U the (π,Q) spiral state is stabilized in a low to intermediate doping range. For large U the (Q,Q) spiral remains the mean-field solution with Q changing more rapidly with doping. The tendency towards phase separation is reduced but not removed with increasing $|t'|$. We have not determined here the complete phase diagram and its evolution with t' but rather we have evaluated the doping dependence of the spiral state parameters at selected values of U/t and t'/t. Explicit numbers are collected in Tables I–IV; some of them will be used in the figures of the subsequent chapters.

III. SUSCEPTIBILITIES OF THE SPIRAL STATE

Contrary to the commensurate SDW state of the Hubbard model at half-filling for which any mixing between the spin and charge channels is absent,[24,31–33] spin and charge excitations are coupled together in the spiral states away from half-filling. Since the formation of the spiral spin structure allows the charge carriers to propagate more freely their kinetic energy gain is intimately related to the magnetic structure tightening spin and charge dynamics closely together. Consequently, we need to determine a 4×4 matrix for the mixed susceptibilities of the charge density and the components of the spin density operators.

For this purpose we define a four-component spin and charge operator[34]

$$S_i^\mu=\frac{1}{2}\sum_{\alpha\beta} c_{i\alpha}^\dagger \sigma_{\alpha\beta}^\mu c_{i\beta}, \tag{10}$$

where σ^μ denotes the Pauli spin matrices, μ taking the values ρ,x,y,z. σ^ρ is defined as the 2×2 unit matrix. We then have to determine the susceptibility matrix

$$\chi^{\alpha\beta}(i,j,t)=i\langle TS_i^\alpha(t)S_j^\beta(0)\rangle. \tag{11}$$

Conveniently, we calculate the susceptibilities in the locally rotated spin reference frame in which the translational invariance is restored. That is, Fourier transforming to momentum space we consider the susceptibility matrix

$$\tilde{\chi}^{\alpha\beta}(\mathbf{q},t)=i\langle T\tilde{S}_{\mathbf{q}}^\alpha(t)\tilde{S}_{-\mathbf{q}}^\beta(0)\rangle \tag{12}$$

for the charge and spin density in terms of the d-fermion operators

$$\tilde{S}_{\mathbf{q}}^\mu=\frac{1}{2N}\sum_{\mathbf{k}}\sum_{\alpha\beta} d_{\mathbf{k}+\mathbf{q},\alpha}^\dagger \sigma_{\alpha\beta}^\mu d_{\mathbf{k},\beta}. \tag{13}$$

The susceptibility matrices $\chi_{\alpha\beta}(i,j,t)$ and $\tilde{\chi}_{\alpha\beta}(i-j,t)$ in the two reference frames are related by

$$\chi^{\alpha\beta}(i,j,t)=\sum_{\sigma_1,\sigma_2} D_{\alpha\sigma_1}(i)\tilde{\chi}^{\sigma_1\sigma_2}(i-j,t)D_{\sigma_2\beta}^{-1}(j) \tag{14}$$

with the rotation matrix

$$\mathbf{D}(i)=\begin{bmatrix}1&0&0&0\\0&\cos\theta_i&0&\sin\theta_i\\0&0&1&0\\0&-\sin\theta_i&0&\cos\theta_i\end{bmatrix}. \tag{15}$$

After Fourier transformation we therefore find for the diagonal dynamical susceptibilities the relations

$$\chi^{\rho\rho}(\mathbf{q},\mathbf{q},\omega)=\tilde{\chi}^{\rho\rho}(\mathbf{q},\omega),$$

$$\chi^{yy}(\mathbf{q},\mathbf{q},\omega)=\tilde{\chi}^{yy}(\mathbf{q},\omega),$$

$$\begin{aligned}\chi^{xx}(\mathbf{q},\mathbf{q},\omega)&=\chi^{zz}(\mathbf{q},\mathbf{q},\omega)\\&=\frac{1}{4}\{\tilde{\chi}^{xx}(\mathbf{q}+\mathbf{Q},\omega)+\tilde{\chi}^{xx}(\mathbf{q}-\mathbf{Q},\omega)\\&\quad+\tilde{\chi}^{zz}(\mathbf{q}+\mathbf{Q},\omega)+\tilde{\chi}^{zz}(\mathbf{q}-\mathbf{Q},\omega)\\&\quad+2i[\tilde{\chi}^{xz}(\mathbf{q}+\mathbf{Q},\omega)-\tilde{\chi}^{xz}(\mathbf{q}-\mathbf{Q},\omega)]\}.\end{aligned} \tag{16}$$

Similar relations hold for the off-diagonal susceptibilities.

We proceed by setting up a generalized RPA procedure for the calculation of the susceptibility matrix $\tilde{\chi}^{\alpha\beta}$ in the rotated reference frame (for a similar derivation and notation see also Ref. 34) using the d-fermion Green's function

$$\tilde{G}_{\alpha\beta}(\mathbf{k},t)=-i\langle Td_{\mathbf{k}\alpha}(t)d_{\mathbf{k}\beta}^\dagger(0)\rangle, \tag{17}$$

which is related to the c-fermion Green's function by the transformation

$$G_{\sigma\sigma'}(i,j,t) = -i\langle T c_{i\sigma}(t) c^{\dagger}_{j\sigma'}(0)\rangle$$

$$= \sum_{\alpha\beta} [e^{-i\sigma_y\theta_i/2}]_{\sigma\alpha} \tilde{G}_{\alpha\beta}(i-j,t) [e^{i\sigma_y\theta_j/2}]_{\beta\sigma'}. \tag{18}$$

$\tilde{G}_{\alpha\beta}$ has to be evaluated for the d-fermion Hamiltonian which is obtained by the unitary transformation Eq. (2)

$$H_d = \sum_{\mathbf{k}\sigma} \epsilon^{+}_{\mathbf{k}} d^{\dagger}_{\mathbf{k}\sigma} d_{\mathbf{k}\sigma} + \sum_{\mathbf{k}\sigma} i\epsilon^{-}_{\mathbf{k}} \sigma d^{\dagger}_{\mathbf{k}\sigma} d_{\mathbf{k}-\sigma}$$

$$+ \frac{U}{N} \sum_{\mathbf{k}\mathbf{k}'\mathbf{q}} d^{\dagger}_{\mathbf{k}'+\mathbf{q}\uparrow} d_{\mathbf{k}'\uparrow} d^{\dagger}_{\mathbf{k}-\mathbf{q}\downarrow} d_{\mathbf{k}\downarrow}, \tag{19}$$

where $\sigma = \pm 1$ for spin-up and spin-down electrons, respectively. After the decoupling of the Hubbard interaction term in Eq. (19) for a ferromagnetic spin alignment the matrix Hartree-Fock Green's function $\tilde{\mathbf{G}}_0$ is given by

$$\tilde{\mathbf{G}}_0(\mathbf{k},\omega) = \begin{bmatrix} \tilde{G}_0^{\uparrow\uparrow}(\mathbf{k},\omega) & \tilde{G}_0^{\uparrow\downarrow}(\mathbf{k},\omega) \\ \tilde{G}_0^{\downarrow\uparrow}(\mathbf{k},\omega) & \tilde{G}_0^{\downarrow\downarrow}(\mathbf{k},\omega) \end{bmatrix}$$

$$= \mathbf{A}^{-}(\mathbf{k}) \tilde{G}_0^{-}(\mathbf{k},\omega) + \mathbf{A}^{+}(\mathbf{k}) \tilde{G}_0^{+}(\mathbf{k},\omega). \tag{20}$$

Here, we have introduced the matrices

$$\mathbf{A}^{\pm}(\mathbf{k}) = \frac{1}{2} \begin{bmatrix} 1 \mp \dfrac{\Delta}{E_{\mathbf{k}}} & \pm i \dfrac{\epsilon^{-}_{\mathbf{k}}}{E_{\mathbf{k}}} \\ \mp i \dfrac{\epsilon^{-}_{\mathbf{k}}}{E_{\mathbf{k}}} & 1 \pm \dfrac{\Delta}{E_{\mathbf{k}}} \end{bmatrix} \tag{21}$$

and the bare, mean-field propagators $\tilde{G}_0^{\pm}$ are given by

$$\tilde{G}_0^{\pm}(\mathbf{k},\omega) = \frac{1 - f^{\pm}_{\mathbf{k}}}{\omega - E^{\pm}_{\mathbf{k}} + i\delta} + \frac{f^{\pm}_{\mathbf{k}}}{\omega - E^{\pm}_{\mathbf{k}} - i\delta}. \tag{22}$$

Using the transformation formula Eq. (18) the diagonal c-fermion Green's functions are expressed in terms of $\tilde{G}_0^{\pm}$ by

$$G_0^{\uparrow\uparrow}(\mathbf{k},\mathbf{k},\omega) = G_0^{\downarrow\downarrow}(\mathbf{k},\mathbf{k},\omega)$$

$$= \tfrac{1}{2} \{ v^2_{\mathbf{k}+\mathbf{Q}/2} \tilde{G}_0^{-}(\mathbf{k}+\mathbf{Q}/2,\omega) + u^2_{\mathbf{k}-\mathbf{Q}/2}$$

$$\times \tilde{G}_0^{-}(\mathbf{k}-\mathbf{Q}/2,\omega) + u^2_{\mathbf{k}+\mathbf{Q}/2} \tilde{G}_0^{+}(\mathbf{k}+\mathbf{Q}/2,\omega)$$

$$+ v^2_{\mathbf{k}-\mathbf{Q}/2} \tilde{G}_0^{+}(\mathbf{k}-\mathbf{Q}/2,\omega) \} \tag{23}$$

with the coherence factors

$$u^2_{\mathbf{k}} = \frac{1}{2}\left[1 + \frac{\epsilon^{-}_{\mathbf{k}}}{E_{\mathbf{k}}}\right], \quad v^2_{\mathbf{k}} = \frac{1}{2}\left[1 - \frac{\epsilon^{-}_{\mathbf{k}}}{E_{\mathbf{k}}}\right]. \tag{24}$$

As is easily verified, for $\mathbf{Q} = (\pi,\pi)$ Eq. (23) reduces to the well known result for the Hartree-Fock Green's function of the commensurate SDW state.[24]

Now we use the Green's function $\tilde{\mathbf{G}}_0$ for the calculation of the bare susceptibilities $\tilde{\chi}_0^{\alpha\beta}$ of the spiral state. (Note that here "spiral" refers to the spin structure in the original reference frame; the d fermions move in a ferromagnetic background. Their momenta extend therefore over the full Brillouin zone and not the reduced magnetic zone.) In the particle-hole single bubble diagrams the 2×2 matrix structure of the d-fermion Green's function is taken into account by allowing for spin flip processes along the d-fermion lines, as shown in Fig. 2 for the diagonal charge-charge and spin-spin susceptibilities. Explicitly, the bare diagonal susceptibilities are calculated from

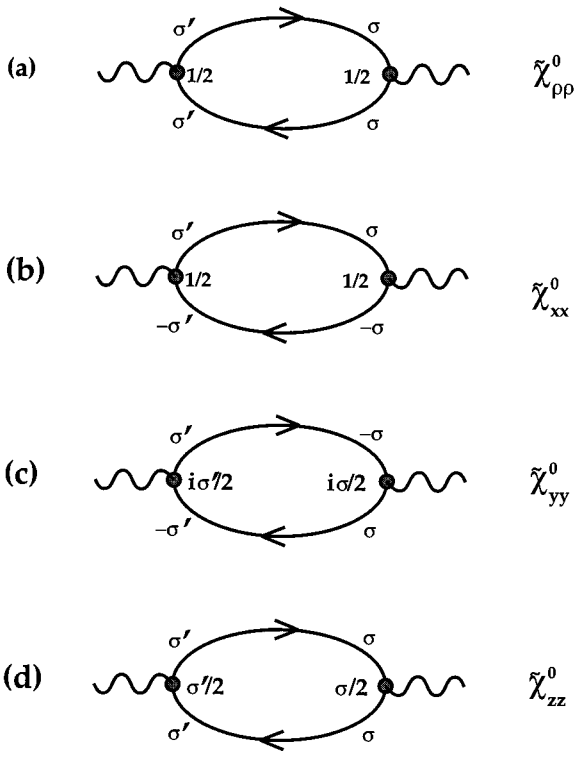

FIG. 2. Bare bubble diagrams for the calculation of the susceptibilities (a) $\tilde{\chi}_0^{\rho\rho}$, (b) $\tilde{\chi}_0^{xx}$, (c) $\tilde{\chi}_0^{yy}$, (d) $\tilde{\chi}_0^{zz}$ in the Hartree-Fock spiral state. The vertices for the charge and the spin components are indicated in the figure.

$$\tilde{\chi}_0^{\rho\rho}(\mathbf{q},\omega) = \frac{i}{4}\frac{1}{N}\sum_{\mathbf{k}} \sum_{\sigma\sigma'} \int \frac{d\nu}{2\pi} \tilde{G}_0^{\sigma\sigma'}(\mathbf{k},\nu) \times \tilde{G}_0^{\sigma'\sigma}(\mathbf{k}+\mathbf{q},\omega+\nu),$$

$$\tilde{\chi}_0^{xx}(\mathbf{q},\omega) = \frac{i}{4}\frac{1}{N}\sum_{\mathbf{k}} \sum_{\sigma\sigma'} \int \frac{d\nu}{2\pi} \tilde{G}_0^{-\sigma-\sigma'}(\mathbf{k},\nu) \times \tilde{G}_0^{\sigma'\sigma}(\mathbf{k}+\mathbf{q},\omega+\nu),$$

$$\tilde{\chi}_0^{yy}(\mathbf{q},\omega) = \frac{i}{4}\frac{1}{N}\sum_{\mathbf{k}} \sum_{\sigma\sigma'} \int \frac{d\nu}{2\pi} (-\sigma\sigma') \times \tilde{G}_0^{\sigma-\sigma'}(\mathbf{k},\nu) \tilde{G}_0^{\sigma'-\sigma}(\mathbf{k}+\mathbf{q},\omega+\nu),$$

$$\tilde{\chi}_0^{zz}(\mathbf{q},\omega) = \frac{i}{4}\frac{1}{N}\sum_{\mathbf{k}} \sum_{\sigma\sigma'} \int \frac{d\nu}{2\pi} \sigma\sigma' \tilde{G}_0^{\sigma\sigma'}(\mathbf{k},\nu) \times \tilde{G}_0^{\sigma'\sigma}(\mathbf{k}+\mathbf{q},\omega+\nu). \tag{25}$$

Similarly to the examples in Fig. 2 we obtain the mixed density and spin susceptibilities. The results for the elements

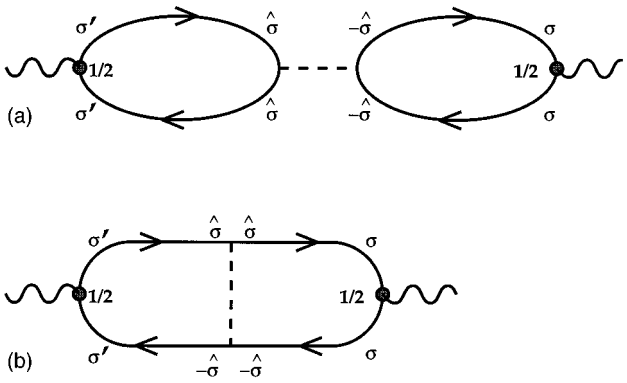

FIG. 3. Leading order bubble (a) and ladder (b) diagrams for the generalized RPA Dyson equation of the dynamical spin and charge susceptibility matrix.

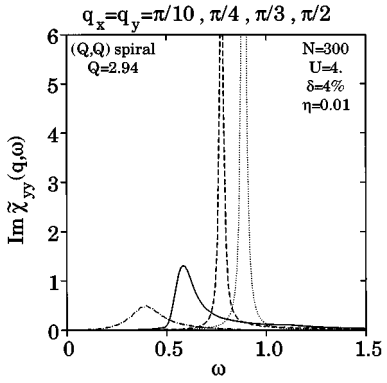

FIG. 4. Imaginary part of the yy-spin susceptibility at low frequencies for four different momenta on the diagonal of the Brillouin zone ($q_x=q_y$): $q_x=\pi/2$ (dotted line), $q_x=\pi/3$ (dashed line), $q_x=\pi/4$ (solid line), and $q_x=\pi/10$ (dashed-dotted line). $\mathrm{Im}\tilde{\chi}^{yy}$ is shown for the diagonal (Q,Q) spiral state in the absence of next-nearest-neighbor hopping $t'=0$ for $U=4t$ and a hole concentration of 4%. The susceptibility has been calculated on a 300×300 sites lattice.

of the bare susceptibility matrix $\tilde{\chi}_0$ are listed in the Appendix obtained by using the vertices indicated in Fig. 2.

IV. COLLECTIVE EXCITATIONS

We account for the residual interactions between the Hartree-Fock quasiparticles by summing the RPA bubble and ladder diagram series. For an outline of the procedure we demonstrate in detail the calculation of the density-density susceptibility. For this purpose we consider first the leading order, linear in U diagrams, i.e., the double-bubble (B1) and the single rung ladder (L1) diagrams as shown in Fig. 3. Explicitly, the evaluation of the two diagrams gives

$$\tilde{\chi}^{\rho\rho}_{B1}(\mathbf{q},\omega)=-2U[\tilde{\chi}^{\rho\rho}_0(\mathbf{q},\omega)\tilde{\chi}^{\rho\rho}_0(\mathbf{q},\omega)-\tilde{\chi}^{\rho z}_0(\mathbf{q},\omega)\tilde{\chi}^{z\rho}_0(\mathbf{q},\omega)],$$

$$\tilde{\chi}^{\rho\rho}_{L1}(\mathbf{q},\omega)=2U[\tilde{\chi}^{\rho x}_0(\mathbf{q},\omega)\tilde{\chi}^{\rho x}_0(\mathbf{q},\omega)+\tilde{\chi}^{\rho y}_0(\mathbf{q},\omega)\tilde{\chi}^{y\rho}_0(\mathbf{q},\omega)]. \quad (26)$$

Therefore, taking the sum of both contributions we obtain to leading order in U (leaving out the arguments of the dynamical susceptibilities for brevity)

$$\tilde{\chi}^{\rho\rho}=\tilde{\chi}^{\rho\rho}_0-2U(\tilde{\chi}^{\rho\rho}_0\tilde{\chi}^{\rho\rho}_0-\tilde{\chi}^{\rho x}_0\tilde{\chi}^{x\rho}_0-\tilde{\chi}^{\rho y}_0\tilde{\chi}^{y\rho}_0-\tilde{\chi}^{\rho z}_0\tilde{\chi}^{z\rho}_0). \quad (27)$$

Proceeding similarly for all mixed density-spin susceptibilities and summing the bubble and ladder diagram series to all orders leads to the Dyson GRPA matrix equation

$$\tilde{\chi}(\mathbf{q},\omega)=\tilde{\chi}_0(\mathbf{q},\omega)-2U\tilde{\chi}_0(\mathbf{q},\omega)\Gamma\tilde{\chi}(\mathbf{q},\omega), \quad (28)$$

where Γ is a diagonal matrix with $\Gamma_{\rho\rho}=1$ and $\Gamma_{xx}=\Gamma_{yy}=\Gamma_{zz}=-1$. The poles of $\tilde{\chi}$ determine the dispersion for the collective mode of the dynamically mixed spin and charge channels.

Equation (28) reduces to the known result for the commensurate SDW state at half-filling with $\mathbf{Q}=(\pi,\pi)$. In this limit the zeroth order susceptibility matrix $\tilde{\chi}_0$ reduces to

$$\tilde{\chi}_0(\mathbf{q},\omega)=\begin{bmatrix}\tilde{\chi}^{\rho\rho}_0 & 0 & 0 & 0\\ 0 & \tilde{\chi}^{xx}_0 & \tilde{\chi}^{xy}_0 & 0\\ 0 & \tilde{\chi}^{yx}_0 & \tilde{\chi}^{yy}_0 & 0\\ 0 & 0 & 0 & \tilde{\chi}^{zz}_0\end{bmatrix}. \quad (29)$$

The spin wave dispersion then follows from the vanishing of the determinant of $\tilde{\chi}$ and is thus determined from the condition

$$(1-2U\tilde{\chi}^{xx}_0)(1-2U\tilde{\chi}^{yy}_0)-4U^2\tilde{\chi}^{xy}_0\tilde{\chi}^{yx}_0=0. \quad (30)$$

Inserting the matrix elements of $\tilde{\chi}_0$ as given in the Appendix it is easily verified that the result agrees with the dispersion derived previously for the SDW state of the half-filled Hubbard model on a square lattice.[24,31] In particular, in the large U limit the dispersion reduces to the linear spin-wave theory results of the AF Heisenberg model with exchange coupling $J=4t^2/U$.

V. RESULTS FOR THE EXCITATION SPECTRUM

We have evaluated the dynamical susceptibilities on finite lattices of up to 400×400 sites. All matrix elements of $\tilde{\chi}$ share the same poles, albeit with different residues, and the spectrum of the collective excitations can be obtained from either the charge or the spin susceptibility. For convenience we have chosen $\tilde{\chi}^{yy}(\mathbf{q},\omega)$ for the evaluation of the collective mode dispersion because $\tilde{\chi}^{yy}$ is identical to $\chi^{yy}(\mathbf{q},\mathbf{q},\omega)$ in the original c-fermion spin reference frame [see Eq. (16)].

Figure 4 shows a representative result for the low frequency range of $\mathrm{Im}\tilde{\chi}^{yy}(\mathbf{q},\omega)$ for the diagonal (Q,Q) spiral state at a hole density of 4% for different momenta along the Brillouin zone diagonal. Spectral weight from excitations between the lower and upper quasiparticle band across the indirect energy gap appears at higher energies. The sharp peaks identify the frequencies of the collective excitation. The peaks become broad for small momenta due to the finite lifetime from the interference with the continuum of particle-

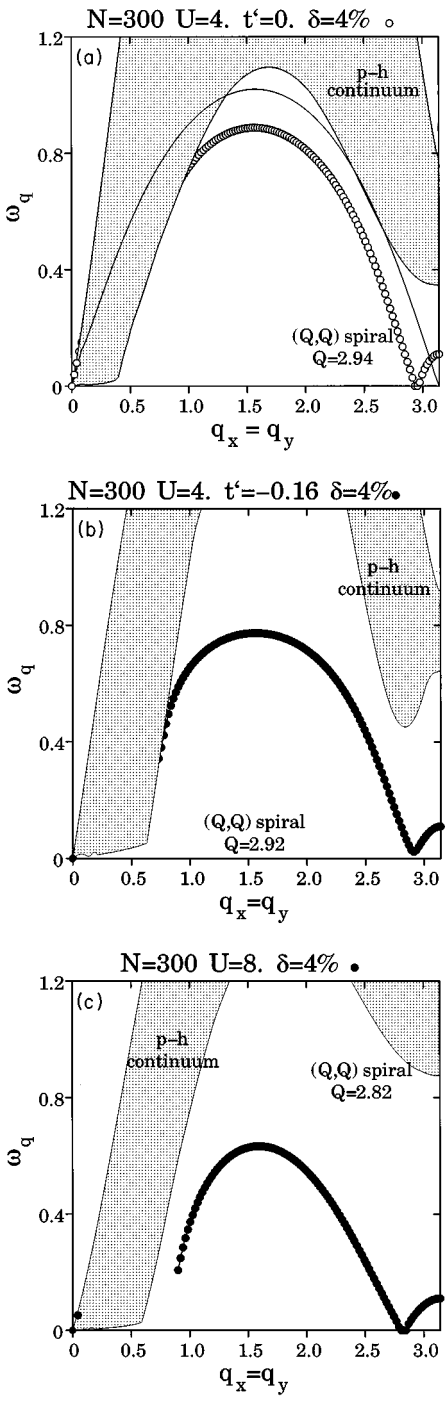

FIG. 5. Collective mode dispersion of the (Q,Q) spiral state along the diagonal of the Brillouin zone at a hole doping of 4% for (a) $U=4t$, $t'=0$, (b) $U=4t$, $t'=-0.16t$, and (c) $U=8t$, $t'=0$. The shaded area represents the continuum of particle-hole excitations in the lower quasiparticle band. In (a) the thin solid line is the spin-wave dispersion in the SDW state at half-filling.

hole (p-h) excitations inside the lower quasiparticle band. Similar spectra are obtained with the inclusion of t' hopping.

In order to determine the dispersion of the collective excitation the peaks in $\mathrm{Im}\tilde{\chi}^{yy}(\mathbf{q},\omega)$ have been traced along different paths in the Brillouin zone. Figure 5 shows the dispersion of the collective mode together with the continuum of intravalence band p-h excitations for the (Q,Q) spiral state at a hole doping of 4% with and without the inclusion of t' hopping for $U=4$ and $U=8$. As expected from the general symmetry arguments (see above) we find a Goldstone mode of the spiral state located at $\mathbf{q}=\mathbf{Q}$. In comparison to the spin-wave spectrum in the SDW state at half-filling the presence of the p-h continuum shifts the collective mode to lower energies in a wide range of momenta. For $U=4$ the collective mode smoothly dissolves into the p-h continuum at longer wavelengths, i.e., the collective mode acquires a finite lifetime due to its decay into p-h excitations. Although barely resolved in the finite size lattice calculations the collective mode reappears above the p-h continuum in the long wavelength $\mathbf{q}\rightarrow 0$ limit; the "spin-wave velocity" near $\mathbf{q}=0$ is thereby enhanced compared to the velocity in the SDW state similarly as in the rigid band picture for the doped commensurate SDW state.[33] This result agrees with Ref. 18 but disagrees with the t-J model calculation of Ref. 17. The small $\mathbf{q}$ part of the dispersion, however, very rapidly dissolves into the p-h continuum with increasing doping.

A different behavior is observed for larger values of U. In this case, instead of dissolving into the p-h continuum, the dispersion surprisingly develops another zero energy mode.[18] This mode is not related to any additional symmetry breaking indicating a dynamical instability of the homogeneous spiral state. In Fig. 5(c) this zero energy mode follows from extrapolating the dispersion above the upper edge of the p-h continuum. The true appearance of a zero-energy mode has been verified by selected calculations on even bigger size lattices. A similar behavior for the collective mode dispersion has recently been observed in the strong coupling functional integral scheme of Zhou and Schulz.[18] However, we emphasize the different behavior at weak and strong coupling as is evident from a comparison of Figs. 5(b) and 5(c).

Similar results are obtained for the collective mode dispersion with finite t' hopping and also in the (π,Q) spiral state which is the mean-field solution at couplings $U/t<10$ in an intermediate hole doping range[8] (see also Tables I–IV). In addition, the modes in the (π,Q) state are damped in even larger regions of the Brillouin zone.

While already the appearance of an additional zero-energy mode at strong coupling indicates a dynamical instability towards an inhomogeneous spiral state, complementary information is obtained from evaluating the static susceptibili-

TABLE I. Mean-field parameters (obtained from minimizing the mean-field energy on a 400×400 lattice) of the spiral state for $t'=0$ and $U=4$ (here and in the subsequent tables energies are given in units of t).

Filling	μ	Q_x	Q_y	m	Energy
1.00	-1.3811	3.1414	3.1416	0.3453	-0.7970
0.98	-1.1938	3.0360	3.0360	0.3298	-0.8111
0.96	-1.0874	2.9463	2.9463	0.3150	-0.8271
0.94	-1.0207	2.8673	2.8673	0.3007	-0.8441
0.92	-0.9776	2.7996	2.7996	0.2866	-0.8613
0.90	-0.9499	2.7413	2.7413	0.2729	-0.8785
0.88	-0.8321	3.1416	2.6174	0.2510	-0.8953
0.86	-0.7891	3.1416	2.5477	0.2357	-0.9139
0.84	-0.7602	3.1416	2.4805	0.2207	-0.9324
0.82	-0.7435	3.1416	2.4168	0.2059	-0.9506

TABLE II. Mean-field parameters (obtained from minimizing the mean-field energy on a 400×400 lattice) of the spiral state for $t'=0$ and $U=8$.

Filling	μ	Q_x	Q_y	m	Energy
1.00	-3.5710	3.1416	3.1416	0.4463	-0.4659
0.98	-3.2130	2.9727	2.9727	0.4345	-0.4775
0.96	-2.9533	2.8216	2.8216	0.4235	-0.4935
0.94	-2.7491	2.6806	2.6806	0.4130	-0.5126
0.92	-2.5921	2.5517	2.5517	0.4030	-0.5337
0.90	-2.4676	2.4317	2.4317	0.3934	-0.5560
0.88	-2.3823	2.3208	2.3208	0.3853	-0.5788
0.86	-2.2950	2.2129	2.2129	0.3751	-0.6018
0.84	-2.2349	2.1121	2.1121	0.3664	-0.6245
0.82	-2.1903	2.0154	2.0154	0.3582	-0.6467

TABLE IV. Mean-field parameters (obtained from minimizing the mean-field energy on a 400×400 lattice) of the spiral state for $t'=-0.16$ and $U=8$.

Filling	μ	Q_x	Q_y	m	Energy
1.00	-3.5710	3.1416	3.1416	0.4464	-0.4659
0.98	-3.2473	2.9540	2.9540	0.4348	-0.4770
0.96	-2.9824	2.7766	2.7766	0.4242	-0.4924
0.94	-2.7651	2.6075	2.6075	0.4145	-0.5110
0.92	-2.5880	2.4449	2.4449	0.4056	-0.5319
0.90	-2.4450	2.2891	2.2891	0.3975	-0.5545
0.88	-2.3262	2.1342	2.1342	0.3902	-0.5781
0.86	-2.2304	1.9826	1.9826	0.3834	-0.6021
0.84	-2.1512	1.8315	1.8315	0.3773	-0.6263
0.82	-2.0915	1.6788	1.6788	0.3716	-0.6503

ties in the vicinity of the Goldstone mode momentum. For this purpose we show in Fig. 6 the inverse of $\tilde{\chi}^{xx}(\mathbf{q},\omega=0)$ and $\tilde{\chi}^{yy}(\mathbf{q},\omega=0)$ in the diagonal spiral state for $\mathbf{q}$ near $\mathbf{Q}$. $\tilde{\chi}^{xx}$ represents spin fluctuations within the plane and $\tilde{\chi}^{yy}$ fluctuations out of the spiral plane. [As a reminder: the coplanar spiral spin order was assumed to be in the x-z plane, $\langle \mathbf{S}_i \rangle = m(\sin\mathbf{Q}\cdot\mathbf{r}_i, 0, \cos\mathbf{Q}\cdot\mathbf{r}_i)$.]

As expected from the presence of the Goldstone mode $\tilde{\chi}^{xx}(\mathbf{q},0)$ and $\tilde{\chi}^{yy}(\mathbf{q},0)$ diverge both at $\mathbf{q}=\mathbf{Q}$, hence their inverse vanishes. Furthermore, the static susceptibility for out-of-plane spin fluctuations, $\tilde{\chi}^{yy}$ is positive for all momenta, not only in the vicinity of $\mathbf{Q}$ as shown in Figs. 6(a) and 6(b), as would be required for a stable state. However, in agreement with the results of Chubukov and Musaelian,[22] the susceptibility for in-plane spin fluctuations (longitudinal fluctuations in their language) is *negative* around the Goldstone mode wave number — a clear second indication that the homogeneous diagonal spiral state is thermodynamically unstable. A similar conclusion was drawn earlier by Dombre in a macroscopic treatment based on the Shraiman/Siggia model.[11] As shown in Fig. 6 this instability occurs at weak as well as strong coupling with and without the inclusion of a finite t' hopping. In contrast to Ref. 22 we find the same instability also for the (π,Q) spiral state (see Fig. 7).[35]

A separate remarkable result is the flatness of $1/\tilde{\chi}^{yy}(\mathbf{q},0)$ for momenta between $\mathbf{q}=\mathbf{Q}$ and $\mathbf{q}=(\pi,\pi)$ along the Brillouin zone diagonal indicating a large susceptibility for out-of-plane spin fluctuations. A similar result has been obtained in the small doping, strong coupling expansion by Chubukov and Musaelian.[22] In their paper the authors find to leading order in the hole concentration δ a whole line of zero energy modes. Higher order terms in δ will still leave a line

TABLE III. Mean-field parameters (obtained from minimizing the mean-field energy on a 400×400 lattice) of the spiral state for $t'=-0.16$ and $U=4$.

Filling	μ	Q_x	Q_y	m	Energy
1.00	-1.3813	3.1416	3.1416	0.3453	-0.7970
0.98	-1.3108	3.0215	3.0215	0.3304	-0.8098
0.96	-1.2648	2.9119	2.9119	0.3170	-0.8229
0.94	-1.2196	3.1416	2.8029	0.3007	-0.8360
0.92	-1.1868	3.1416	2.7043	0.2870	-0.8491
0.90	-1.1596	3.1416	2.6122	0.2737	-0.8621
0.88	-1.1381	3.1416	2.5251	0.2607	-0.8747
0.86	-1.1189	3.1416	2.4434	0.2482	-0.8870
0.84	-1.1035	3.1416	2.3675	0.2361	-0.8988
0.82	-1.0869	3.1416	2.2981	0.2240	-0.9100

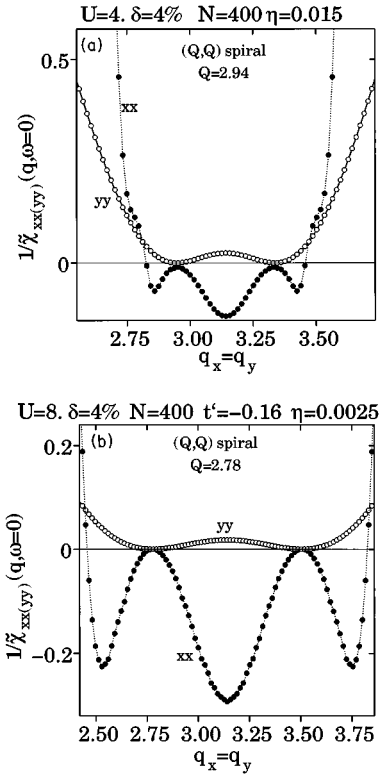

FIG. 6. Inverse of the static susceptibilities $\tilde{\chi}^{xx}(\mathbf{q})$ and $\tilde{\chi}^{yy}(\mathbf{q})$ for in-plane and out-of-plane spin fluctuations of the planar diagonal spiral, respectively, in the neighborhood of the Goldstone mode wave number $\mathbf{Q}=(Q,Q)$. The figures demonstrate the same behavior at weak and strong coupling with and without next-nearest-neighbor hopping. The different parameter sets are indicated in the figure. δ is the hole concentration, N the linear lattice size, and $i\eta$ is an artificially introduced broadening for the energy denominators of the susceptibilities.

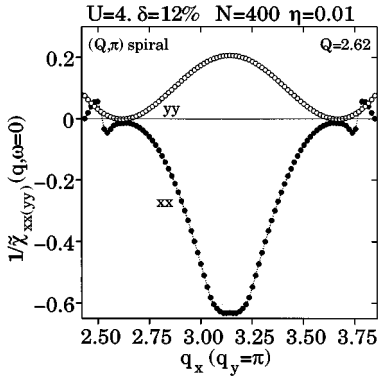

FIG. 7. Same as in Fig. 6 for the (Q,π) spiral showing the same behavior for in-plane spin fluctuations with a negative $\tilde{\chi}^{xx}(\mathbf{q},0)$ near (π,π).

of near-zero energy modes and it is argued that these modes indicate the indifference of the coplanar spiral towards generation of a spontaneous staggered magnetization in the out-of-plane direction while the incommensurate order in the spiral plane is maintained. In order to examine this suggestion we extend the calculations presented so far to the case of noncoplanar spiral states.

VI. NONCOPLANAR SPIRAL STATES

We generalize the class of spiral states by allowing for an additional out-of-plane (i.e., y-direction) component of the magnetization. In order to perform the mean-field calculation as done above for a ferromagnetic spin alignment we apply a second transformation and locally rotate the spin quantization axis for the d fermions by an angle φ_i around the x axis (alternatively we can perform a rotation around the z axis). We therefore introduce p-fermion operators by

$$p_{i\sigma}=\sum_{\tilde{\sigma}} [e^{i\varphi_i\sigma_x/2}]_{\sigma\tilde{\sigma}} d_{i\tilde{\sigma}}. \tag{31}$$

The two subsequent local rotations Eqs. (2) and (31) transform the eigenvectors of the Pauli spin matrix σ_z into the eigenvectors along the local quantization axis specified by the spherical angle $\Omega_i=(\theta_i,\varphi_i)$. The unitary transformations change the kinetic energy part of the Hamiltonian into

$$H_{\mathrm{kin}}=-\sum_{ij}\sum_{\sigma\tilde{\sigma}} t_{ij}T^{ij}_{\sigma\tilde{\sigma}}p^{\dagger}_{i\sigma}p_{j\tilde{\sigma}}+\mathrm{H.c.} \tag{32}$$

The form of the Hubbard interaction remains unchanged as before. In Eq. (32) we have defined the matrix

$$\mathbf{T}^{ij}=\begin{bmatrix} \cos\frac{\theta_{ij}}{2}\cos\frac{\varphi_{ij}}{2}-i\sin\frac{\theta_{ij}}{2}\sin\frac{\varphi_i+\varphi_j}{2} & \sin\frac{\theta_{ij}}{2}\cos\frac{\varphi_i+\varphi_j}{2}+i\cos\frac{\theta_{ij}}{2}\sin\frac{\varphi_{ij}}{2} \\ -\sin\frac{\theta_{ij}}{2}\cos\frac{\varphi_i+\varphi_j}{2}+i\cos\frac{\theta_{ij}}{2}\sin\frac{\varphi_{ij}}{2} & \cos\frac{\theta_{ij}}{2}\cos\frac{\varphi_{ij}}{2}+i\sin\frac{\theta_{ij}}{2}\sin\frac{\varphi_i+\varphi_j}{2} \end{bmatrix}, \tag{33}$$

with $\varphi_{ij}=\varphi_i-\varphi_j$. From the appearance of the sum of the angles $\varphi_i+\varphi_j$ in the components of the matrix $\mathbf{T}_{ij}$ it follows that the system is in general no longer translational invariant. However, for the special case of a staggered out-of-plane magnetization, i.e., if

$$\varphi_i=\varphi e^{i(\pi,\pi)\cdot\mathbf{r}_i} \tag{34}$$

and hence $\varphi_i+\varphi_j=0$ for nearest-neighbor sites i,j, the translational invariance is restored. In this case we obtain for the kinetic energy after Fourier transformation

$$H_{\mathrm{kin}}=\sum_{\mathbf{k},\sigma}(A_{\mathbf{k}}p^{\dagger}_{\mathbf{k},\sigma}p_{\mathbf{k},\sigma}+i\sigma B_{\mathbf{k}}p^{\dagger}_{\mathbf{k},\sigma}p_{\mathbf{k},-\sigma} +iC_{\mathbf{k}}p^{\dagger}_{\mathbf{k},\sigma}p_{\mathbf{k}-(\pi,\pi),-\sigma}+\sigma D_{\mathbf{k}}p^{\dagger}_{\mathbf{k},\sigma}p_{\mathbf{k}-(\pi,\pi),\sigma}). \tag{35}$$

In Eq. (35) we have defined the coefficients

$$A_{\mathbf{k}}=\cos\varphi\,\epsilon^{+}_{\mathbf{k}}(t,t'=0)+\epsilon^{+}_{\mathbf{k}}(t=0,t'),$$

$$B_{\mathbf{k}}=-[\epsilon^{-}_{\mathbf{k}}(t,t'=0)+\cos\varphi\,\epsilon^{-}_{\mathbf{k}}(t=0,t')],$$

$$C_{\mathbf{k}}=-\sin\varphi\,\epsilon^{+}_{\mathbf{k}}(t,t'=0),$$

$$D_{\mathbf{k}}=-\sin\varphi\,\epsilon^{-}_{\mathbf{k}}(t=0,t'). \tag{36}$$

For $\varphi_i\equiv 0$ we recover the kinetic energy in Eq. (19).

Again we follow the same route for the mean-field decoupling of the Hubbard interaction assuming now a ferromagnetic order in the p-fermion spin reference frame. The diagonalization of the mean-field Hamiltonian is now a 4×4 problem leading to four quasiparticle bands in the reduced Brillouin zone [defined by the momenta for which $\epsilon_{\mathbf{k}}(t,t'=0)\leq 0$]. For $t'=0$ the four bands have the dispersions

$$E^{\pm\pm}_{\mathbf{k}}=\pm\sqrt{(\epsilon^{+}_{\mathbf{k}}\cos\varphi)^2+E^2_{\mathbf{k}}+(\epsilon^{+}_{\mathbf{k}}\sin\varphi)^2\pm 2\sqrt{(\epsilon^{+}_{\mathbf{k}}\cos\varphi)^2E^2_{\mathbf{k}}+(\epsilon^{-}_{\mathbf{k}}\epsilon^{+}_{\mathbf{k}}\sin\varphi)^2}}, \tag{37}$$

where, as before, $E_{\mathbf{k}}=\sqrt{(\epsilon_{\mathbf{k}}^{-})^2+\Delta^2}$.

For $t'=0$ we have minimized the resulting mean-field energy with respect to the magnetization, the spiral wave number $\mathbf{Q}=(Q_x,Q_y)$, and the staggered angle φ. For the wide parameter range we have explored it is found that the staggered noncoplanar spiral state with a finite φ is *never* the lowest energy mean-field solution. This agrees with the conclusions drawn in Ref. 18. The planar spiral is favored over the noncoplanar spiral state, although the energy differences are very small, characteristically on the per mill level. This near degeneracy with noncoplanar spiral states explains the large static out-of-plane susceptibility of the coplanar spiral states for $\mathbf{q}$ near (π,π). We have not explored the effect of t'-hopping. But due the similar behavior of the static susceptibilities with and without t' a staggered out-of-plane magnetization is not expected in this case either. Unresolved remains the possibility that inhomogeneous noncoplanar states are the favorable mean-field solutions.

VII. SUMMARY AND CONCLUSIONS

In this paper we have presented a calculational scheme for the collective excitations in homogeneous spiral states of the Hubbard model. Although we have focused here on the results for a square lattice, the generalized RPA is naturally applicable for other lattices as well; only the free tight binding dispersion $\epsilon(\mathbf{k})$ has to be replaced accordingly to analyze different lattices in two dimensions (2D) or 3D. For example, an application to the case of the spiral, metallic state in $V_{2-y}O_3$ is planned for future work.

On the square lattice away from half-filling we find in agreement with Ref. 18 that among the homogeneous states coplanar spirals are favored against noncoplanar spirals on the mean-field level, although noncoplanar states are nearly degenerate in energy. In contrast to the commensurate SDW state the spin and charge dynamics are inherently coupled in the spiral state and the mixed spin and charge susceptibilities have to be treated on equal footing. The symmetry breaking in the spiral states leads to three collective Goldstone modes at the wave numbers $\mathbf{q}=\mathbf{0},\pm\mathbf{Q}$. The dispersion of the modes is strongly renormalized by low-energy particle-hole excitations which in addition lead to damping in wide regions of the Brillouin zone with increasing hole doping.

Several signals for the instability of homogeneous spiral states on the square lattice have been identified. Besides the negative mean-field compressibility, the static susceptibility for in-plane spin fluctuations is negative near $\mathbf{q}=(\pi,\pi)$, an even stronger signature for an instability. Surprisingly, an extra zero energy mode appears at strong coupling which is not related to any additional symmetry breaking. Phase separation, domain wall, soliton, or vortex lattice[12] formation for the doped square lattice Hubbard model remain open possibilities, as underlined by the rich variety of inhomogeneous structures found in unrestricted Hartree-Fock calculations.[36] Yet, stable homogeneous spiral states may be realized for other lattice structures[37] and the GRPA serves as a convenient framework to analyze the dynamical spin and charge susceptibilities and will thereby allow also the calculation of the optical conductivity from its relation to the density-density response function.[34]

ACKNOWLEDGMENTS

A.P.K. gratefully acknowledges support of the Deutsche Forschungsgemeinschaft (DFG) and the Sonderforschungsbereich 341 of the DFG.

APPENDIX: RESULTS FOR $\tilde{\chi}_0(\mathbf{Q},\omega)$

In this appendix we evaluate the matrix elements of the bare, mean-field susceptibility matrix $\tilde{\chi}^0$ of the Hartree-Fock spiral state. Inserting the result for the d-fermion Green's function matrix we calculate the bare particle-hole bubble diagrams as shown, e.g., for the diagonal charge-charge and spin-spin susceptibilities in Fig. 1. Introducing

$$\begin{aligned} g^{mn}&\equiv g^{mn}(\mathbf{k},\mathbf{q},\omega)\\ &=\frac{(1-f^m_{\mathbf{k}})f^n_{\mathbf{k}+\mathbf{q}}}{\omega-E^n_{\mathbf{k}+\mathbf{q}}+E^m_{\mathbf{k}}-i\delta}\\ &\quad-\frac{f^m_{\mathbf{k}}(1-f^n_{\mathbf{k}+\mathbf{q}})}{\omega-E^n_{\mathbf{k}+\mathbf{q}}+E^m_{\mathbf{k}}+i\delta} \end{aligned} \tag{A1}$$

for $m,n=\pm$ we find for the components of the 4×4 susceptibility matrix $\tilde{\chi}^{\alpha\beta}$ by following the standard diagrammatic rules:

$$\tilde{\chi}_0^{\rho\rho}(\mathbf{q},\omega)=\frac{1}{4N}\sum_{\mathbf{k}}\{[g^{++}+g^{--}]l^2(\mathbf{k},\mathbf{k}+\mathbf{q})+[g^{+-}+g^{-+}]p^2(\mathbf{k},\mathbf{k}+\mathbf{q})\},$$

$$\tilde{\chi}_0^{\rho x}(\mathbf{q},\omega)=\frac{i}{8N}\sum_{\mathbf{k}}\left\{[g^{++}+g^{--}-g^{+-}-g^{-+}]\times\Delta\frac{\epsilon^{-}_{\mathbf{k}}-\epsilon^{-}_{\mathbf{k}+\mathbf{q}}}{E_{\mathbf{k}}E_{\mathbf{k}+\mathbf{q}}}\right\},$$

$$\tilde{\chi}_0^{\rho y}(\mathbf{q},\omega)=\frac{1}{8N}\sum_{\mathbf{k}}\left\{[g^{--}-g^{++}]\left(\frac{\epsilon^{-}_{\mathbf{k}}}{E_{\mathbf{k}}}+\frac{\epsilon^{-}_{\mathbf{k}+\mathbf{q}}}{E_{\mathbf{k}+\mathbf{q}}}\right)+[g^{-+}-g^{+-}]\left(\frac{\epsilon^{-}_{\mathbf{k}}}{E_{\mathbf{k}}}-\frac{\epsilon^{-}_{\mathbf{k}+\mathbf{q}}}{E_{\mathbf{k}+\mathbf{q}}}\right)\right\},$$

$$\tilde{\chi}_0^{\rho z}(\mathbf{q},\omega)=\frac{1}{4N}\sum_{\mathbf{k}}\{[g^{--}-g^{++}]lm(\mathbf{k},\mathbf{k}+\mathbf{q})+[g^{-+}-g^{+-}]pn(\mathbf{k},\mathbf{k}+\mathbf{q})\},$$

$$\tilde{\chi}_0^{xx}(\mathbf{q},\omega)=\frac{1}{4N}\sum_{\mathbf{k}}\{[g^{++}+g^{--}]p^2(\mathbf{k},\mathbf{k}+\mathbf{q})+[g^{+-}+g^{-+}]l^2(\mathbf{k},\mathbf{k}+\mathbf{q})\},$$

$$\tilde{\chi}_0^{yy}(\mathbf{q},\omega)=\frac{1}{4N}\sum_{\mathbf{k}}\{[g^{++}+g^{--}]n^2(\mathbf{k},\mathbf{k}+\mathbf{q})+[g^{+-}+g^{-+}]m^2(\mathbf{k},\mathbf{k}+\mathbf{q})\},$$

$$\tilde{\chi}_0^{zz}(\mathbf{q},\omega)=\frac{1}{4N}\sum_{\mathbf{k}}\{[g^{++}+g^{--}]m^2(\mathbf{k},\mathbf{k}+\mathbf{q})+[g^{+-}+g^{-+}]n^2(\mathbf{k},\mathbf{k}+\mathbf{q})\},$$

$$\tilde{\chi}_0^{xy}(\mathbf{q},\omega)=\frac{i}{4N}\sum_{\mathbf{k}}\{[g^{--}-g^{++}]pn(\mathbf{k},\mathbf{k}+\mathbf{q})+[g^{-+}-g^{+-}]lm(\mathbf{k},\mathbf{k}+\mathbf{q})\},$$

$$\tilde{\chi}_0^{xz}(\mathbf{q},\omega)=\frac{i}{8N}\sum_{\mathbf{k}}\left\{[g^{++}-g^{--}]\left(\frac{\epsilon_{\mathbf{k}}^{-}}{E_{\mathbf{k}}}-\frac{\epsilon_{\mathbf{k}+\mathbf{q}}^{-}}{E_{\mathbf{k}+\mathbf{q}}}\right)+[g^{+-}-g^{-+}]\left(\frac{\epsilon_{\mathbf{k}}^{-}}{E_{\mathbf{k}}}+\frac{\epsilon_{\mathbf{k}+\mathbf{q}}^{-}}{E_{\mathbf{k}+\mathbf{q}}}\right)\right\},$$

$$\tilde{\chi}_0^{yz}(\mathbf{q},\omega)=\frac{1}{8N}\sum_{\mathbf{k}}\left\{[g^{++}+g^{--}-g^{+-}-g^{-+}]\times\Delta\frac{\epsilon_{\mathbf{k}}^{-}+\epsilon_{\mathbf{k}+\mathbf{q}}^{-}}{E_{\mathbf{k}}E_{\mathbf{k}+\mathbf{q}}}\right\}. \tag{A2}$$

The remaining elements of the 4×4 susceptibility matrix follow from the relations

$$\tilde{\chi}_0^{x\rho}(\mathbf{q},\omega)=-\tilde{\chi}_0^{\rho x}(\mathbf{q},\omega),\quad \tilde{\chi}_0^{y\rho}(\mathbf{q},\omega)=\tilde{\chi}_0^{\rho y}(\mathbf{q},\omega),$$

$$\tilde{\chi}_0^{z\rho}(\mathbf{q},\omega)=\tilde{\chi}_0^{\rho z}(\mathbf{q},\omega),\quad \tilde{\chi}_0^{yx}(\mathbf{q},\omega)=-\tilde{\chi}_0^{xy}(\mathbf{q},\omega),$$

$$\tilde{\chi}_0^{zx}(\mathbf{q},\omega)=-\tilde{\chi}_0^{xz}(\mathbf{q},\omega),\quad \tilde{\chi}_0^{zy}(\mathbf{q},\omega)=\tilde{\chi}_0^{yz}(\mathbf{q},\omega). \tag{A3}$$

In the above expressions for the susceptibility matrix elements we have introduced the coherence factors:

$$p^2(\mathbf{k},\mathbf{k}+\mathbf{q})=\frac{1}{2}\left(1-\frac{\Delta^2+\epsilon_{\mathbf{k}}^{-}\epsilon_{\mathbf{k}+\mathbf{q}}^{-}}{E_{\mathbf{k}}E_{\mathbf{k}+\mathbf{q}}}\right),$$

$$l^2(\mathbf{k},\mathbf{k}+\mathbf{q})=\frac{1}{2}\left(1+\frac{\Delta^2+\epsilon\mathbf{k}^{-}\epsilon_{\mathbf{k}+\mathbf{q}}^{-}}{E_{\mathbf{k}}E_{\mathbf{k}+\mathbf{q}}}\right),$$

$$n^2(\mathbf{k},\mathbf{k}+\mathbf{q})=\frac{1}{2}\left(1-\frac{\Delta^2-\epsilon_{\mathbf{k}}^{-}\epsilon_{\mathbf{k}+\mathbf{q}}^{-}}{E_{\mathbf{k}}E_{\mathbf{k}+\mathbf{q}}}\right),$$

$$m^2(\mathbf{k},\mathbf{k}+\mathbf{q})=\frac{1}{2}\left(1+\frac{\Delta^2-\epsilon_{\mathbf{k}}^{-}\epsilon_{\mathbf{k}+\mathbf{q}}^{-}}{E_{\mathbf{k}}E_{\mathbf{k}+\mathbf{q}}}\right),$$

$$lm(\mathbf{k},\mathbf{k}+\mathbf{q})=\frac{1}{2}\left(\frac{\Delta}{E_{\mathbf{k}}}+\frac{\Delta}{E_{\mathbf{k}+\mathbf{q}}}\right),$$

$$pn(\mathbf{k},\mathbf{k}+\mathbf{q})=\frac{1}{2}\left(\frac{\Delta}{E_{\mathbf{k}}}-\frac{\Delta}{E_{\mathbf{k}+\mathbf{q}}}\right). \tag{A4}$$

At half-filling, with $f_{\mathbf{k}}^{-}\equiv1$ and $f_{\mathbf{k}}^{+}\equiv0$, the results agree with Coté and Tremblay.[34] (Note, however, that in Ref. 34 the susceptibilities have been defined with the opposite sign.)

[1] B.I. Shraiman and E. Siggia, Phys. Rev. Lett. **61**, 467 (1988); **62**, 1564 (1989); Phys. Rev. B **40**, 9162 (1989).
[2] C. Jayaprakash, H.T. Krishnamurthy, and S. Sarker, Phys. Rev. B **40**, 2610 (1989).
[3] C.L. Kane, P.A. Lee, T.K. Ng, B. Chakraborty, and N. Read, Phys. Rev. B **41**, 2653 (1990).
[4] B. Chakraborty, N. Read, C. Kane, and P.A. Lee, Phys. Rev. B **42**, 4819 (1990).
[5] S. John, P. Voruganti, and W. Goff, Phys. Rev. B **43**, 13 365 (1991).
[6] S. Sarker, C. Jayaprakash, H.R. Krishnamurthy, and W. Wenzel, Phys. Rev. B **43**, 8775 (1991).
[7] R. Fresard, M. Dzierzawa, and P. Wölfle, Europhys. Lett. **15**, 325 (1991); R. Fresard and P. Wölfle, J. Phys. Condens. Matter **4**, 3625 (1992).
[8] M. Dzierzawa, Z. Phys. B **86**, 49 (1992).
[9] A. Auerbach and B.E. Larson, Phys. Rev. B **43**, 7800 (1991).
[10] E. Arrigoni and G.C. Strinati, Phys. Rev. B **44**, 7455 (1991).
[11] T. Dombre, J. Phys. (France) **51**, 847 (1990).
[12] M. Ichimura, M. Fujita, and K. Nakao, J. Phys. Soc. Jpn. **61**, 2027 (1992).
[13] H.J. Schulz, J. Phys. (France) **50**, 2833 (1988).
[14] P. Chandra, P. Coleman, and A.I. Larkin, J. Phys. Condens. Matter **2**, 7933 (1990).
[15] E. Rastelli, L. Reatto, and A. Tassa, J. Phys. C **18**, 353 (1985).
[16] B.I. Shraiman and E. Siggia, Phys. Rev. B **46**, 8305 (1992).
[17] J. Gan, N. Andrei, and P. Coleman, J. Phys. Condens. Matter **3**, 3537 (1991).
[18] C. Zhou and H.J. Schulz, Phys. Rev. B **52**, 11 557 (1995).
[19] S.W. Cheong, G. Aeppli, T.E. Mason, H. Mook, S.M. Hayden, P.C. Canfield, Z. Fisk, K.N. Clausen, and J.L. Martinez, Phys. Rev. Lett. **67**, 1791 (1991); T.E. Mason, G. Aeppli, and H.A. Mook, *ibid.* **68**, 1414 (1992); T.E. Mason, G. Aeppli, S.M. Hayden, A.P. Ramirez, and H.A. Mook, *ibid.* **71**, 919 (1993).
[20] W. Bao, C. Broholm, S.A. Carter, T.F. Rosenbaum, G. Aeppli, S.F. Trevino, P. Metcalf, J.M. Honig, and J. Spalek, Phys. Rev. Lett. **71**, 766 (1993).
[21] J. Inoue and S. Maekawa, Phys. Rev. Lett. **74**, 3407 (1995).
[22] A.V. Chubukov and K.A. Musaelian Phys. Rev. B **51**, 12 605 (1995).
[23] H.Q. Lin and J.E. Hirsch, Phys. Rev. B **35**, 3359 (1987).
[24] J.R. Schrieffer, X.G. Wen, and S.C. Zhang, Phys. Rev. B **39**, 11 663 (1989).
[25] H.J. Schulz, Phys. Rev. Lett. **65**, 2462 (1990).
[26] See also A. Auerbach, *Interacting Electrons and Quantum Magnetism* (Springer, New York, 1994), p. 40.
[27] A.P. Kampf and W. Brenig, J. Low Temp. Phys. **95**, 335 (1994); W. Brenig, *ibid.* **99**, 319 (1995).
[28] T. Tohyama and S. Maekawa, Phys. Rev. B **49**, 3596 (1994).
[29] J. Altmann, W. Brenig, A.P. Kampf, and E. Müller-Hartmann, Phys. Rev. B **52**, 7395 (1995).
[30] For recent reviews, see E. Dagotto, Rev. Mod. Phys. **66**, 763 (1994); A.P. Kampf, Phys. Rep. **249**, 219 (1994); W. Brenig, *ibid.* **251**, 153 (1995).
[31] A. Singh and Z. Tešanović, Phys. Rev. B **41**, 614 (1990).

[32] A. Vignale and M.R. Hedayati, Phys. Rev. B **42**, 786 (1990).
[33] A.V. Chubukov and D.M. Frenkel, Phys. Rev. B **46**, 11 884 (1992).
[34] R. Coté and A.-M.S. Tremblay, Europhys. Lett. **29**, 37 (1995).
[35] The negative stiffness near $\mathbf{q}=(\pi,\pi)$ for longitudinal spin fluctuations in the (Q,π) spiral state becomes positive for sufficiently large t' hopping. But, then the stiffness turns negative in a different momentum range.
[36] A.R. Bishop, F. Guinea, P.S. Lomdahl, E. Louis, and J.A. Vergés, Europhys. Lett. **14**, 2 (1991); F. Guinea, E. Louis, and J.A. Vergés, Phys. Rev. B **45**, 4752 (1992).
[37] T. Hanisch, B. Kleine, A. Ritzl, and E. Müller-Hartmann, Ann. Phys. (Leipzig) **4**, 303 (1995).